JCB Report

βIVΣ1 spectrin stabilizes the nodes of Ranvier and axon initial segments

Sandra Lacas-Gervais,[1] Jun Guo,[3] Nicola Strenzke,[4] Eric Scarfone,[5] Melanie Kolpe,[1] Monika Jahkel,[2] Pietro De Camilli,[3] Tobias Moser,[4] Matthew N. Rasband,[6] and Michele Solimena[1]

[1]Experimental Diabetology and [2]Department of Psychiatry, University of Technology Dresden, 01307 Dresden, Germany
[3]Department of Cell Biology and Howard Hughes Medical Institute, Yale University, New Haven, CT 06510
[4]Department of Otolaryngology, University of Goettingen, 37075 Goettingen, Germany
[5]Centre de Recherches de Biochimie Macromoléculaire, Centre National de la Recherche Scientifique, 34293 Montpellier, France
[6]Department of Neurosciences, University of Connecticut, Farmington, CT 06030

Saltatory electric conduction requires clustered voltage-gated sodium channels (VGSCs) at axon initial segments (AIS) and nodes of Ranvier (NR). A dense membrane undercoat is present at these sites, which is thought to be key for the focal accumulation of channels. Here, we prove that βIVΣ1 spectrin, the only βIV spectrin with an actin-binding domain, is an essential component of this coat. Specifically, βIVΣ1 coexists with βIVΣ6 at both AIS and NR, being the predominant spectrin at AIS. Removal of βIVΣ1 alone causes the disappearance of the nodal coat, an increased diameter of the NR, and the presence of dilations filled with organelles. Moreover, in myelinated cochlear afferent fibers, VGSC and ankyrin G clusters appear fragmented. These ultrastructural changes can explain the motor and auditory neuropathies present in βIVΣ1 −/− mice and point to the βIVΣ1 spectrin isoform as a master-stabilizing factor of AIS/NR membranes.

Introduction

Saltatory electric conduction in myelinated neurons relies on the compartmentalized distribution of ion channels along the axons. Voltage-gated sodium channels (VGSCs), in particular, are clustered at axon initial segments (AIS) and nodes of Ranvier (NR), whereas potassium channels reside in the juxtaparanodes, which are separated from the NR by the interposition of the paranodes (Poliak and Peles, 2003; Salzer, 2003). Opening of VGSCs at AIS and NR triggers the generation and regeneration of action potentials, respectively. Changes in the expression and/or localization of proteins enriched at AIS/NR, paranodes, and juxtaparanodes affect nerve conduction and cause neuropathies (Suter and Scherer, 2003).

Since their first description by electron microscopy (Robertson, 1957), it has been appreciated that NR display distinctive structural properties, including a thick coat beneath the plasma membrane, which most likely reflects the assembly of cytoskeletal proteins involved in the clustering of VGSCs. Recent studies have shown that anchoring of sodium channels to the cortical actin cytoskeleton is mediated by the binding of their cytoplasmic tail to ankyrins and spectrins. Originally discovered in erythrocytes, ankyrins (Bennett and Stenbuck, 1979) and spectrins (Marchesi and Steers, 1968) are now clearly appreciated as key organizers and scaffolding components of membrane microdomains in virtually all cells, including neurons (Bennett and Baines, 2001). Increasing evidence points to spectrins as also having a role in membrane trafficking (De Matteis and Morrow, 2000).

βIV spectrin was recently identified as the specific spectrin found at AIS and NR (Berghs et al., 2000), where it interacts with VGSCs through its binding to ankyrin G 480/270 (Jenkins and Bennett, 2001; Komada and Soriano, 2002). Alternative splicing generates six βIV spectrin isoforms (βIVΣ1–βIVΣ6; see Fig. 1 A; Berghs et al., 2000; Tse et al., 2001, Komada and Soriano, 2002). Genetic removal of multiple βIV spectrins in mice reduces immunoreactivity for ankyrin G and VGSCs at AIS and NR (Komada and Soriano, 2002). These mice display tremors, clasping of the hind limbs, and altered gait, consistent with a decreased nerve conductivity. A similar phenotype is present in the various

Address correspondence to M. Solimena, Medical School, University of Technology Dresden, Fetscherstrasse, 74, 01307 Dresden, Germany. Tel.: 49-351-4586611. Fax: 49-351-4586330.
email: michele.solimena@mailbox.tu-dresden.de

Key words: cytoskeleton; deafness; sciatic nerve; cochlea; cerebellum

Abbreviations used in this paper: ABR, auditory brainstem responses; AIS, axon initial segments; CNS, central nervous system; NR, nodes of Ranvier; PNS, peripheral nervous system; SD, specific domain; VGSC, voltage-gated sodium channel.

The Journal of Cell Biology
http://www.jcb.org/cgi/doi/10.1083/jcb.200408007

"quivering" mouse strains, each arising from spontaneous mutations in the βIV spectrin gene causing progressively longer truncations of βIV spectrins (Parkinson et al., 2001). Preliminary evidence suggested that βIVΣ1 and a 140-kD βIV spectrin (Berghs et al., 2000, 2001), conceivably βIVΣ6 (Komada and Soriano, 2002), are found at AIS and NR, whereas βIVΣ5 is in the nucleus (Tse et al., 2001). Accordingly, it is still unclear how many βIV spectrin isoforms are found at AIS and NR. Identification of these isoforms and of the isoforms whose absence is responsible for the phenotypes in βIV spectrin-deficient mice may help to elucidate which interactions of spectrin are most critical for its function at AIS and NR.

Here, we prove that βIVΣ1 and βIVΣ6 are present at both central and peripheral AIS and NR and that absence of βIVΣ1 alone destabilizes AIS/NR generating a quivering phenotype. Moreover, our data highlight the physiological relevance of βIVΣ1 in the myelinated afferent fibers of the auditory pathway, which innervate the sensory hair cells.

Results and discussion

Generation of βIVΣ1 spectrin −/− mice

Exon 2 of mouse βIV spectrin, which encodes the first methionine, was removed by homologous recombination (Fig. 1 B). PCR analyses confirmed the targeting of βIV spectrin in heterozygous (+/−) and homozygous mutant (−/−) mice (Fig. 1 C). βIVΣ1 −/− mice were born with Mendelian frequency, but were smaller than +/+ and +/− littermates (weight at 3 wk: +/+, 13.2 ± 0.8 g, $n = 5$; +/−, 12.4 ± 0.7 g, $n = 21$, $P < 0.01$; −/−, 10.0 ± 0.6 g, $n = 4$; $P < 0.05$) and displayed tremors, mild dysmetria, clumsy gait, and dragging of the hind limbs. Despite these deficits, 3- and 5-mo-old βIVΣ1 −/− mice scored like +/+ mice

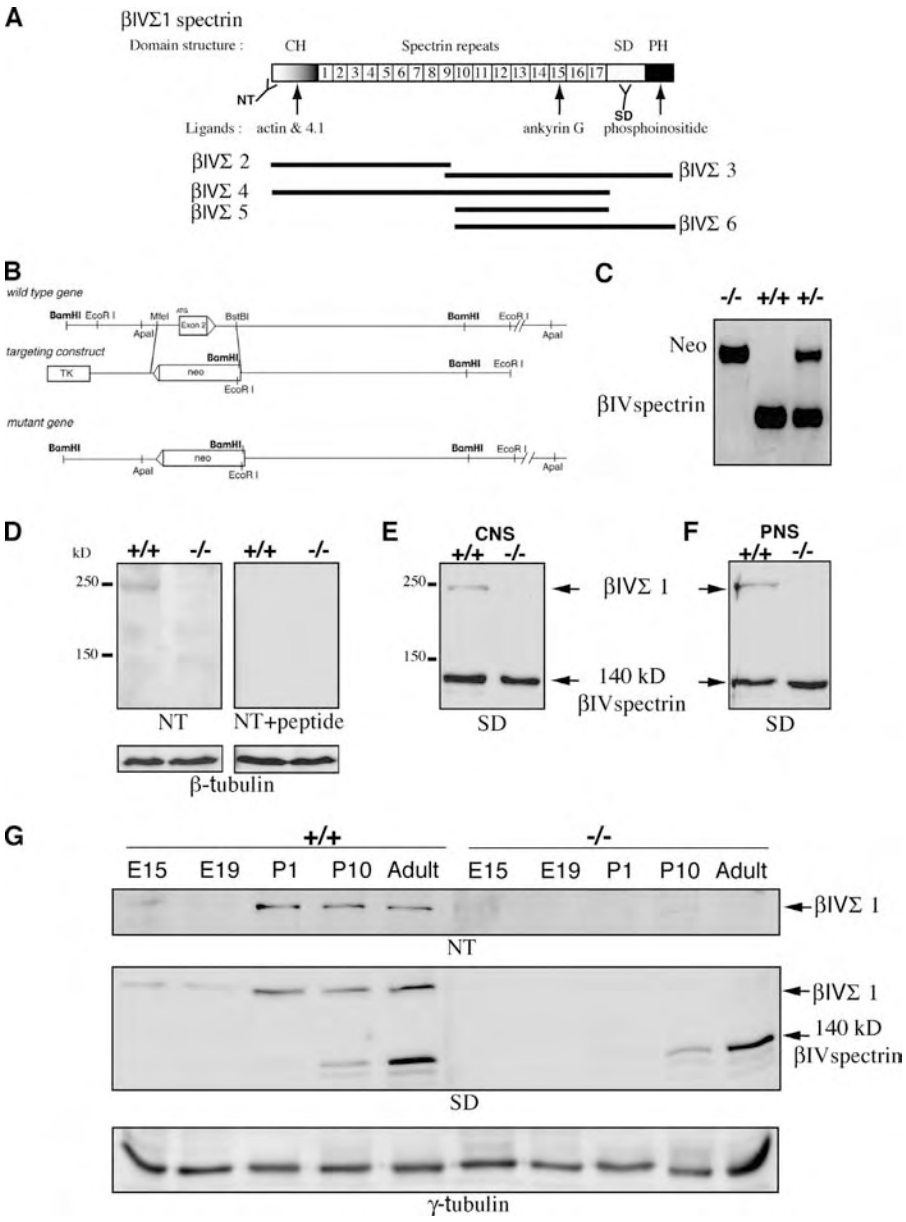

Figure 1. **Generation of βIVΣ1 −/− mice.** (A) Schematic view of βIV spectrins. The domain structure of βIVΣ1, including binding sites and regions recognized by the NT and SD antibodies, is shown in detail. The other βIV spectrins are shown with black lines. CH, calponin homology domain; SD, specific domain; PH, pleckstrin homology domain. (B) Construct for the deletion of exon 2 of βIV spectrin. (C) Genotyping of βIVΣ1 +/+, +/−, and −/− mice by PCR using primers for exon 2 of βIV spectrin (150 bp product) and *neo* (310 bp product). (D–F) Immunoblots on brain (D and E) and sciatic nerve (F) extracts from adult βIVΣ1 +/+ and −/− mice with the NT (D) or SD (E and F) antibodies. The right panel in D shows the immunoblot with the NT antibody preincubated with its antigenic peptide. Protein loading in D was verified by immunoblotting for β-tubulin. (G) Levels of βIV spectrins, as detected by the NT and SD antibodies, at embryonic days 15 (E15) and 19 (E19), postnatal days 1 (P1) and 10 (P10), and adults. Protein loading was checked by immunoblotting for γ-tubulin, which is not developmentally regulated.

for their running wheel activity for 1 h (unpublished data) or open field locomotion for 20 min (distance covered, number of rearing, and time at rest; unpublished data). Their lifespan was normal and no abnormalities were found by pathological survey of multiple organs, including the brain (unpublished data).

Immunoblot with two antibodies confirmed the deletion of βIVΣ1. The NT antibody binds an NH_2-terminal epitope in βIVΣ1, βIVΣ2, and βIVΣ4, whereas the specific domain (SD) antibody binds the domain unique to βIVΣ1, βIVΣ3, and βIVΣ6 (Fig. 1 A). In +/+ mouse brain, the NT antibody detected a single protein of 250 kD (Fig. 1 D), corresponding to βIVΣ1 (Berghs et al., 2000). This reactivity was absent in βIVΣ1 −/− mice and was abolished by preincubating the antibody with its immunogenic peptide. Notably, the NT antibody did not detect other isoforms besides βIVΣ1. Thus, the expression in vivo of βIVΣ2 and βIVΣ4 remains to be proven. The SD antibody also did not detect βIVΣ1 in −/− mice, while its reactivity with βIVΣ6 was unaffected (Fig. 1 E). As in rat (Berghs et al., 2000), βIVΣ1 was already present in mouse embryonic brain, whereas βIVΣ6 only appeared after birth (Fig. 1 G). Notably, in the absence of βIVΣ1 there was no temporal or quantitative compensatory expression of βIVΣ6.

Coexistence of βIVΣ1 and βIVΣ6 at AIS and NR, with predominance of βIVΣ1 at AIS

The expression of βIVΣ1 during development suggested that this isoform plays a role at AIS, which are formed before NR. The postnatal appearance of βIVΣ6 parallels myelination and the progressive creation of NR. Presence of βIVΣ1 and βIVΣ6 in sciatic nerves, which include NR but no AIS, indicated that both isoforms are at NR (Fig. 1 F).

The NT antibody, which only binds βIVΣ1, stained AIS (Fig. 2, A and C, arrowheads) and NR (Fig. 2, A and C, arrows) in the cerebellum of +/+ mice (Fig. 2, A and C), but not in −/− mice (Fig. 2, B and D). This staining was blocked by the antigenic peptide and was not detected with the secondary antibody alone (unpublished data). These data prove that βIVΣ1 is found in both AIS and NR. The SD antibody labeled more intensively AIS and NR of +/+ mice than the NT antibody (Fig. 2 E), partly because it recognizes also βIVΣ6. In βIVΣ1 −/− mice, the SD labeling was reduced (Fig. 2, F and H) but not abolished, indicating that βIVΣ6 coexists with βIVΣ1 at AIS and NR. This labeling was more strongly reduced at AIS (Fig. 2, G and H, arrowheads) than at NR (Fig. 2 G and H, arrows), suggesting that βIVΣ1 is the major spectrin at AIS. This hypothesis was corroborated by evidence that in βIVΣ1 +/+ mice AIS were already visible at postnatal day 1 (P1; Fig. 2 I), whereas

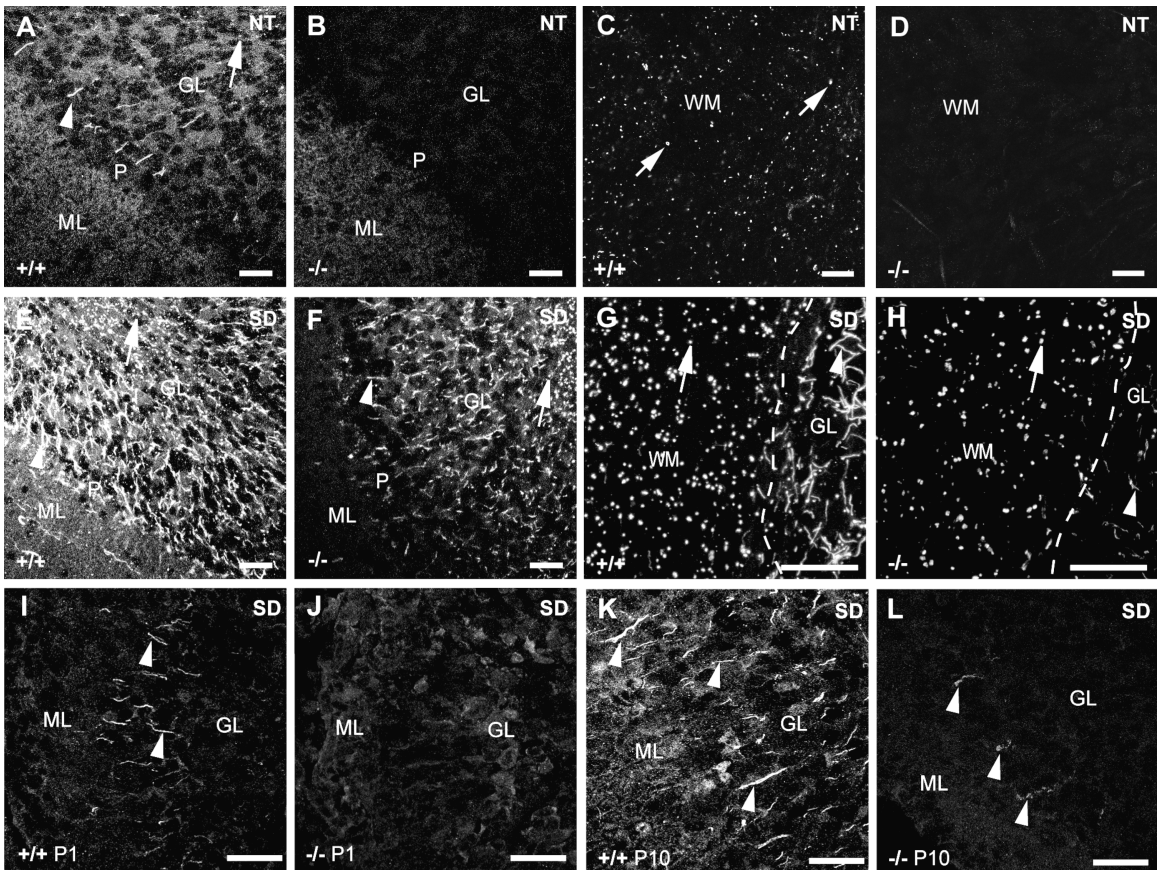

Figure 2. **Staining for βIV spectrin in βIVΣ1 +/+ and −/− mice.** Confocal images of cerebellar sections from adult (A–H), 1- (P1, I and J), or 10-d-old (P10, K and L) mice labeled with the NT (A–D) and SD (E–L) antibodies. The dashed lines in G and H show the boundary between the white matter (WM), where NR are found, and the granular layer (GL), where AIS predominate. Arrowheads, AIS; arrows, NR; ML, molecular layer; P, Purkinje cells. Bars, 25 μm.

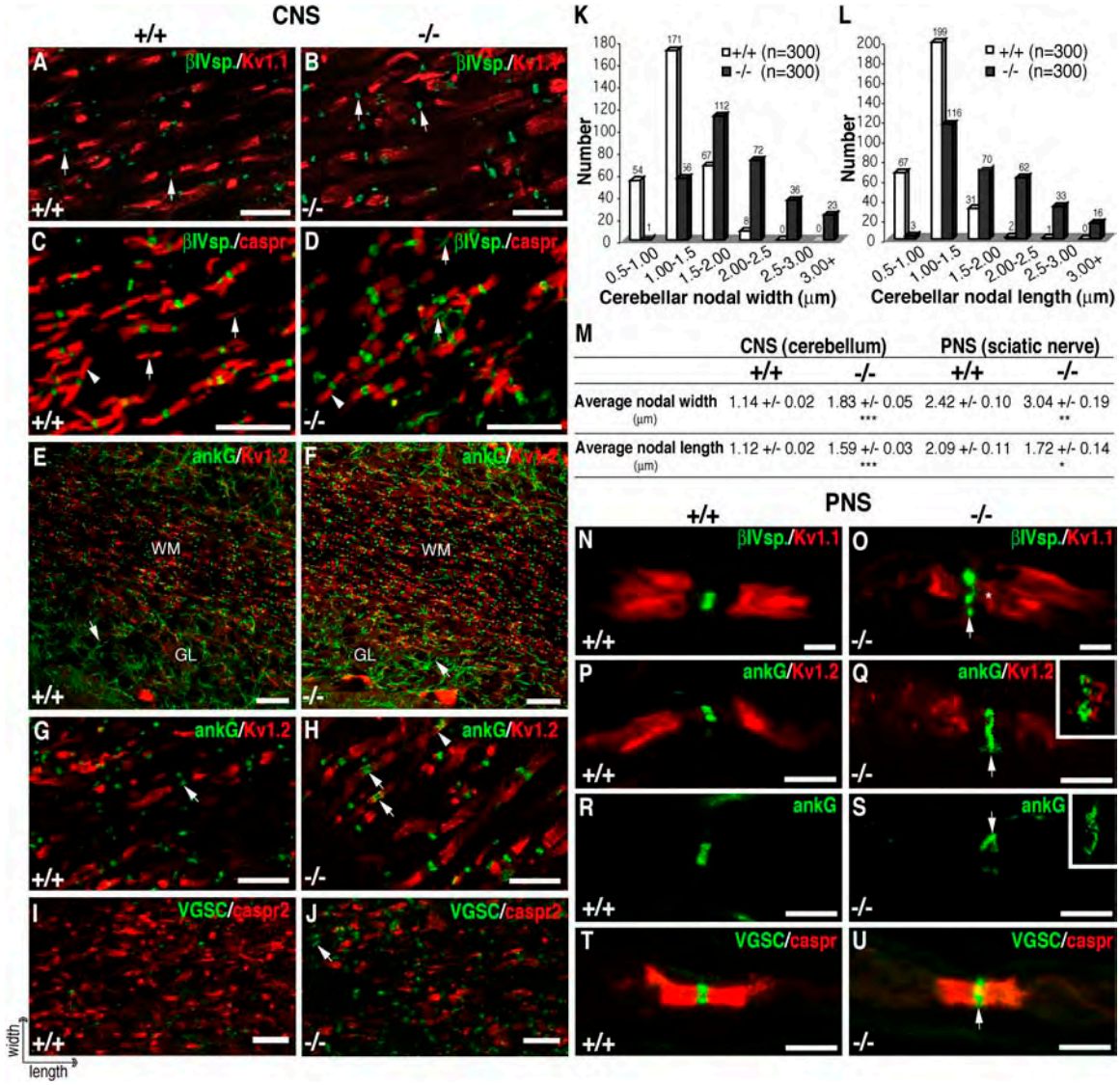

Figure 3. **Distribution of nodal markers in the CNS and PNS of βIVΣ1 +/+ and −/− mice.** (A–J) Cerebellar sections of βIVΣ1 +/+ and −/− mice were double labeled as indicated for the following proteins: βIV spectrin (βIV sp.; SD antibody), Kv1.1, caspr/paranodin (caspr), ankyrin G (ankG), Kv1.2, VGSCs, and caspr2. The arrows in A–D, G, and H point to NR in axons of comparable size. (K and L) Graphic representation of the width (K) and length (L) of NR in the CNS of βIVΣ1 +/+ and −/− mice. Measurements were from images of sections labeled for βIV spectrin, ankyrin G, and VGSCs. 100 NR for each labeling and phenotype (total = 300 NR/phenotype) were measured. Values were binned into 0.5-μm increments. The orientation of the axes referred to as width and length is shown at the bottom left of panel I. (M) Average width and length of 100 cerebellar and 22 sciatic NR/phenotype, as measured on images of VGSCs. Data are presented as mean ± SEM. *, $P \leq 0.05$; **, $P \leq 0.01$; ***, $P \leq 0.001$. (N–U) Sections of sciatic nerve from βIVΣ1spectrin +/+ and −/− mice single or double stained for the indicated proteins. The arrows in O, Q, S, and U point to NR in βIVΣ1 −/− mice. In O, an asterisk indicates the invasion of a paranode by Kv.1.1. In Q and S, the insets (2× magnification relative to P–S) show additional shorter and wider NR in βIVΣ1 −/− mice. GL, granular layer; WM, white matter. Bars: (A–D and G– J) 10 μm; (E and F) 25 μm; (N–U) 5 μm.

in βIVΣ1 −/− mice, which still express βIVΣ6, they were only detected at P10 (Fig. 2 L), and more weakly than in +/+ mice (Fig. 2, L vs. K). As βIVΣ6 was still found at AIS and NR in the absence of βIVΣ1, whereas βIV spectrins were absent in AIS of Purkinje cells lacking ankyrin G (Jenkins and Bennett, 2001), it is conceivable that nodal targeting of βIV spectrins depends on their binding to ankyrin G.

Altered shape of NR in βIVΣ1 −/− mice

Next, we examined if βIVΣ1 is required for the integrity of central nervous system (CNS) and peripheral nervous system (PNS) nodes, as well as for the distribution of various markers in this compartment. Labeling of the cerebellum with SD (Fig. 3, A–D), anti-ankyrin G (Fig. 3, E–H), or anti-VGSCs (Fig. 3, I and J) antibodies showed that nodal width and length were increased in βIVΣ1 −/− (Fig. 3 M, $P \leq 0.001$): 81% (243/300) of the NR in βIVΣ1 −/− mice had a width >1.5 μm, compared with 25% (75/300) in +/+ mice (Fig. 3 K), whereas the length of 60% of the NR in βIVΣ1 −/− mice was >1.5 μm, compared with 11% in +/+ mice (Fig. 3 L). The labeling for ankyrin G (Fig. 3, E and F) and VGSCs (not depicted) at AIS was

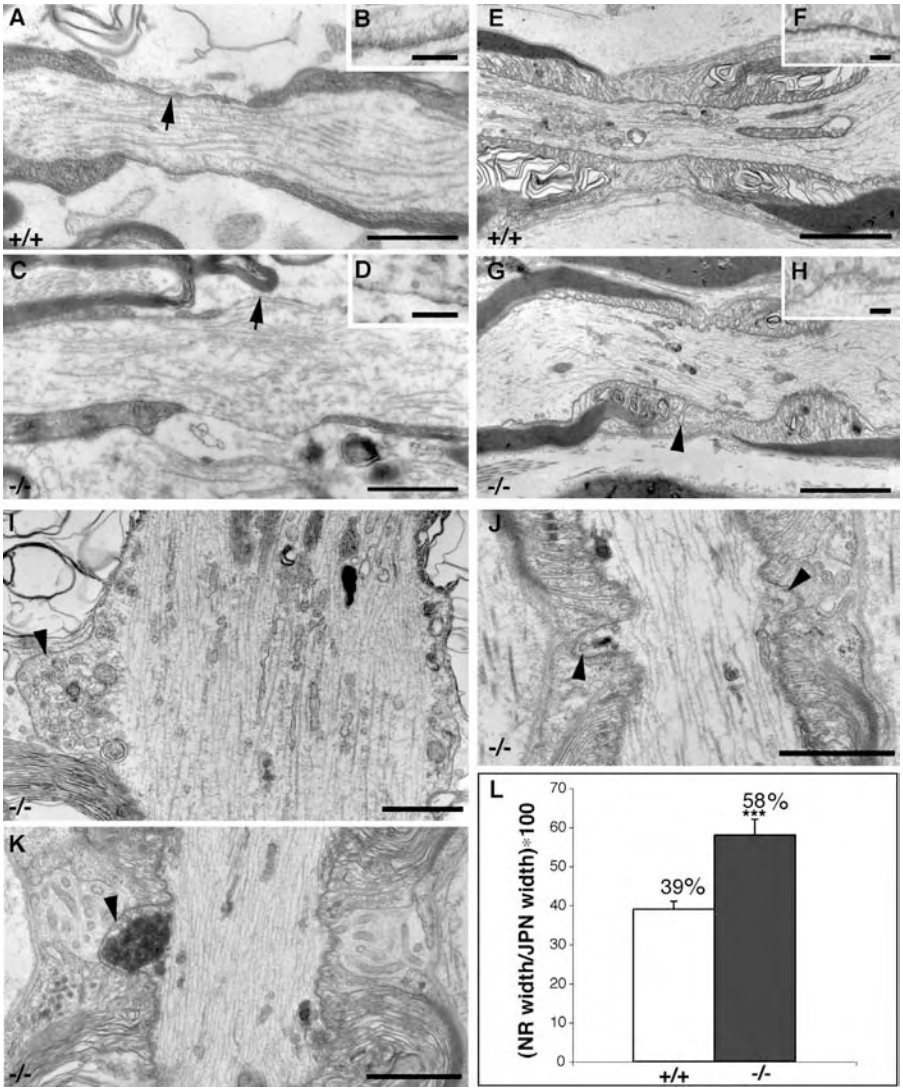

Figure 4. **Ultrastructure of CNS and PNS NR in βIVΣ1 +/+ and −/− mice.** EM of the optic (A–D) and sciatic (E–K) nerves from adult βIVΣ1 +/+ (A, B, E, and F) and −/− mice (C, D, and G–K). Arrows and insets show the coat beneath the NR membrane. Arrowheads show the protrusions in the NR of βIVΣ1 −/− mice. (L) Ratio between the width of each NR and its corresponding juxtaparanodes. Errors are given as mean ± SEM. ***, $P < 0.001$. Bars: (A, C, and I–K) 1 μm; (E and G) 2 μm; (B, D, F and H) 125 nm.

brighter and thicker in βIVΣ1 −/− (Fig. 3, arrows in F vs. E). Because by immunoblot the levels of ankyrin G and VGSCs were not changed (unpublished data), the increased immunoreactivity may result from an enhanced accessibility of these antigens to antibodies in the absence of βIVΣ1. According to this interpretation, βIVΣ1, similar to βIVΣ6 (Komada and Soriano, 2002), binds ankyrin G through its repeat 15 and thereby to VGSCs.

Changes were also found in the paranodes and juxtaparanodes of βIVΣ1 −/− mice. The labeling for the paranodal marker caspr/paranodin was equally intense in βIVΣ1 −/− mice as in +/+ mice, but the length of the paranodes was reduced (Fig. 3, D vs. C, arrowheads). In βIVΣ1 −/− mice, the staining for potassium channels Kv1.1 (Fig. 3, B vs. A) and Kv1.2 (Fig. 3, H vs. G), which are normally restricted to the juxtaparanodes, was decreased and more spread, albeit the total reactivity for Kv1.1 was similar (average optical density: βIVΣ1 +/+, 0.242 ± 0.0002 vs. βIVΣ1 −/−, 0.244 ± 0.0004). Occasionally, Kv1.2 immunoreactivity invaded the paranodes (Fig. 3 H, arrowhead). Similar observations were made in the optic nerve (unpublished data). An altered distribution of Kv channels has also been observed in the quivering *qv*^{jnd} mouse (Parkinson et al., 2001). As βIV spectrin is not detected at paranodes and juxtaparanodes, such changes can indirectly result from the alterations at the NR.

The NR in the sciatic nerves of βIVΣ1 −/− mice were shorter, larger, and geometrically less regular than in +/+ mice (Fig. 3, N–U). Measurement of 22 NR/genotype confirmed that in βIVΣ1 −/− mice their width was increased ($P \leq 0.01$), while their length was reduced ($P \leq 0.05$; Fig. 3 M). Absence of βIVΣ1 caused also alterations of the PNS paranodes and juxtaparanodes. The caspr labeling was less compact and could invade the NR (Fig. 3, U vs. T). Likewise, Kv1.1 and Kv1.2 were less clustered at juxtaparanodes (Fig. 3, Q vs. P) and could invade the paranodes (Fig. 3, O vs. N, asterisk). However, by immunoblot the levels of VGSCs and Kv1.2 were not changed (unpublished data). Thus, also in the PNS the lack of βIVΣ1 changed the pattern of nodal and juxtaparanodal markers.

Ultrastructural abnormalities of NR in βIVΣ1 −/− mice

To conclusively prove the occurrence of structural alterations in the absence of βIVΣ1, NR in the optic (CNS) and sciatic (PNS) nerves of βIVΣ1 +/+ and −/− mice were examined by electron microscopy. NR in the optic nerve of −/− mice were longer and swollen (Fig. 4, C vs. A), whereas

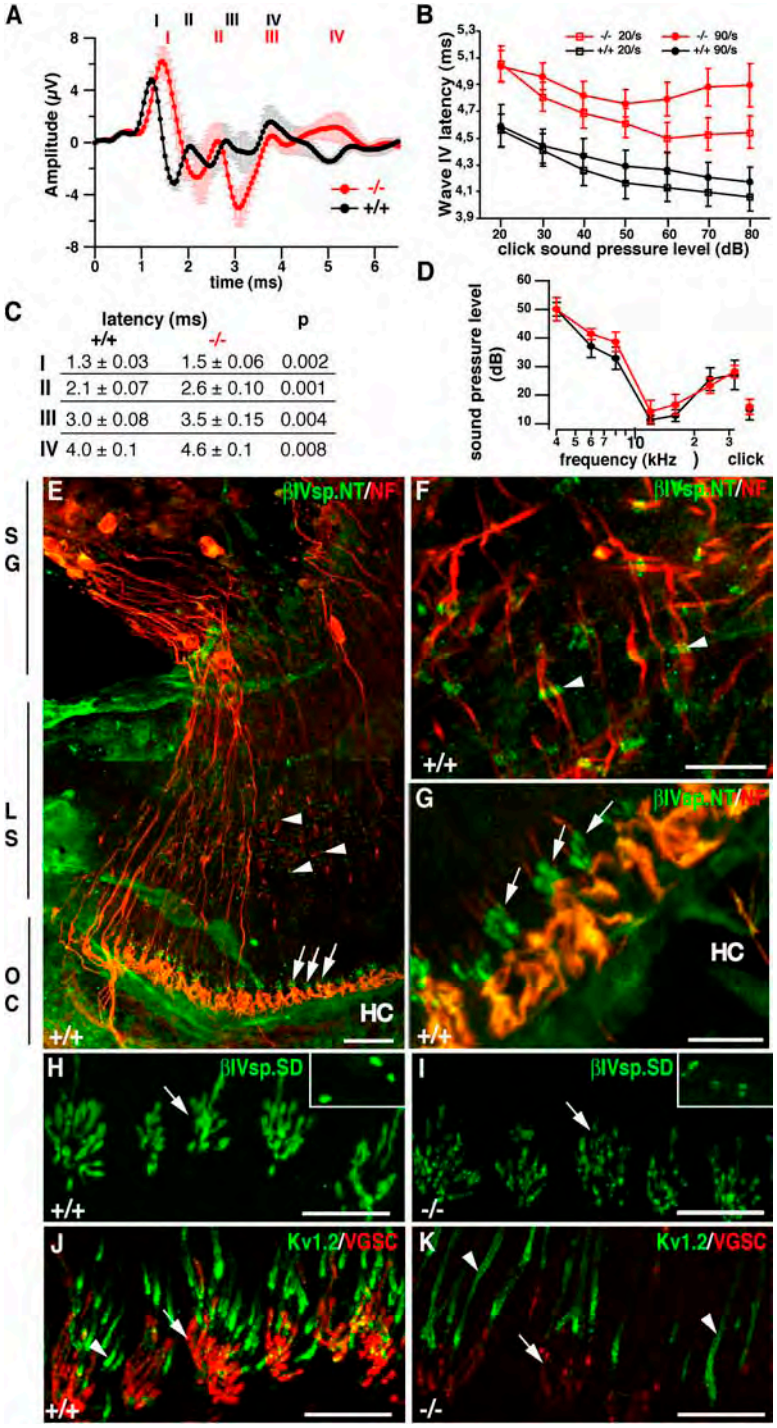

Figure 5. **βIVΣ1 spectrin in the auditory pathway.** (A) ABR recorded from βIVΣ1 +/+ (black line, $n = 5$) and −/− (red line, $n = 5$) mice upon stimulation with 80-dB clicks with error bars in voltage (SEM of the grand average). Roman numbers indicate the ABR peaks as described previously (Jewett et al., 1970). (B) Latencies of ABR waves IV (mean ± SEM from four βIVΣ1 +/+ and five βIVΣ1 −/− mice) after stimulation with 20 or 90 clicks per second as a function of intensity (20–80 dB SPL peak equivalent). The increase in latencies at the higher stimulation rate was significant ($P < 0.05$, paired t test) for all values between 30 and 80 dB in βIVΣ1 −/− mice. (C) Mean latencies recorded from five βIVΣ1 +/+ and five −/− mice. The mean latencies in βIVΣ1 −/− mice were longer (unpaired t test). (D) Averaged hearing thresholds (dB SPL) determined at various frequencies in βIVΣ1 +/+ (black line) and −/− (red line) mice ($n = 7$ for both groups, $n = 5$ for clicks). (E–K) Staining of cochlear afferent fibers in βIVΣ1 +/+ and −/− mice. (E) View of the cochlea in βIVΣ1 +/+ mice. The neurofilament staining (NF; red) shows the cell bodies of sensory neurons in the spiral ganglion (SG), the bundles of afferent fibers running through the Lamina Spiralis (LS), and the terminals of these fibers in the organ of Corti (OC), where they innervate hair cells (HC). βIVΣ1 is stained with the NT antibody (green). HC are not visible. The hazy green background is due to the thickness of the specimen. Arrows and arrowheads (E–G) point to AIS and NR-like structures along afferent fibers, respectively. (F and G) Higher magnification of NR and AIS-like structures in LS and OC, respectively. (H–K) AIS and NR-like structures (H and I, insets) along afferent fibers stained with SD (H and I) and VGSCs/Kv1.2 (J and K) in the OC from βIVΣ1 +/+ and −/− mice. Bars: (E) 30 μm; (F–K) 10 μm.

the electron dense membrane undercoat was absent (Fig. 4, C vs. A, arrows; and D vs. B). Ultrastructural changes were also observed in peripheral NR of βIVΣ1 −/− mice (Fig. 4, G–K). Their length was reduced (Fig. 4, G vs. E), whereas lateral protrusions, which were never detected in +/+ mice, were found in 7/15 NR (Fig. 4, G and I–K, arrowheads). Large evaginations often contained vesicles (Fig. 4, I–K), some with an electron-dense core. Except within these dilations, the NR of βIVΣ1 −/− mice contained fewer vesicles. Normally there is a higher density of vesicles at NR than at internodal regions, possibly because the nodal restriction slows axonal transport (Zimmermann, 1996). Consistently, vesicle density may be reduced in βIVΣ1 −/− mice because NR are enlarged (see the following paragraph).

The membrane coat was also reduced in the NR of sciatic nerves (Fig. 4, H vs. F). As axons vary in diameter, the ratio between the diameter of each NR and their corresponding juxtaparanodes was calculated. This analysis showed that the diameter of NR in βIVΣ1 −/− mice was 58 ± 4% of the corresponding juxtaparanode diameter, compared with 39 ± 2% in +/+ mice ($P \leq 0.001$; Fig. 3 L). This increase of ∼20% is consistent with the enlargement of ∼25% assessed on confocal images. Conversely, axoglial junctions at the paranodes of βIVΣ1 −/− mice appeared normal (unpub-

lished data). Notably, even if βIVΣ6 is expressed at higher levels than βIVΣ1, it is not sufficient to stabilize the structure of AIS and NR, conceivably because βIVΣ6, unlike βIVΣ1, lacks the NH_2-terminal actin/protein 4.1 binding domain and is therefore less suited to anchor ankyrin G and surface proteins to the cortical cytoskeleton.

Auditory neuropathies in βIVΣ1 −/− mice

The quivering phenotype and the alterations at AIS and NR suggested that nerve conduction is affected in βIVΣ1 −/− mice. As auditory neuropathies are part of the quivering phenotype, auditory brainstem responses (ABR), were measured. ABR allow the assessment of hearing acuity by measuring the brain waves generated along the auditory pathway in response to acoustic stimuli. Unlike spontaneous quivering mice (Parkinson et al., 2001), βIVΣ1 −/− mice displayed ABR (Fig. 5 A), but the latency of their auditory evoked potentials was increased (Fig. 5 C). Raising the stimulation rate further increased these latencies (Fig. 5 B), indicating an auditory neural fatigue. This deficit can reflect a delayed generation of action potentials by cochlear spiral ganglion neurons and an impaired conduction along the auditory pathway. A deficit of sensory hair cells can be excluded, as auditory thresholds were not changed (Fig. 5 D). This interpretation is consistent with the enrichment of βIVΣ1 at sites where the afferent fibers of the spiral ganglion sensory neurons leave the organ of Corti and become myelinated (Fig. 5, E and G, arrows). Therefore, these sites, where action potentials are thought to originate, can functionally equal the AIS in multipolar neurons. Likewise, the sites where βIVΣ1 clusters along myelinated afferent fibers (Fig. 5, E and F, arrowheads) can be equaled to the NR.

In βIVΣ1 −/− mice, stainings for βIV spectrin (Fig. 5, I vs. H and insets I vs. H), VGSCs (Fig. 5, K vs. J), and ankyrin G (not depicted) at both these sites were reduced and fragmented, whereas Kv1.2 was more spread (Fig. 5, K vs. J). Notably, each AIS-equivalent site was still positive for βIV spectrin, albeit the residual staining was altered. These data prove that βIVΣ1 and βIVΣ6 coexists at each AIS and that βIVΣ1 plays a key role in stabilizing the AIS structure. Our analyses extend those performed previously (Parkinson et al., 2001), as βIVΣ1 −/− mice not only display prolonged latencies of ABR, but also suffer from auditory fatigue, which is a hallmark of neural hearing impairment (Hood, 1950). In general, the altered electrical conduction and axonal membrane trafficking resulting from the molecular and ultrastructural changes reported here may both contribute to the quivering features of βIVΣ1 −/− mice, including ataxic tremor and auditory neuropathy.

In conclusion, our data provide a definitive molecular correlate to the membrane undercoat at NR. Specifically, they prove that βIVΣ1 is a major component of the nodal cortical coat and that in its absence the plastic properties of the nodal membrane are impaired. The scaffolding role of spectrins is known from the seminal studies in erythrocytes (Marchesi, 1985; Bennett and Baines, 2001), yet no formal proof for any spectrin isoform having this role in neuron has been provided before. This knowledge may open new opportunities for the understanding of axonal physiology in normal and pathological conditions.

Materials and methods

Generation of βIVΣ1 spectrin −/− mice

Plasmids from a C57BL mouse BAC library (Genome Systems Inc.) were isolated by screenings with a mouse βIV spectrin cDNA probe and digested with multiple restriction enzymes. Two fragments of 5.6 and 8.4 Kb including exon 2 of βIV spectrin were used to generate a construct, in which a 600-bp fragment containing exon 2 was replaced with PMC1-*neo* gene in the opposite orientation. The construct included a 5′-genomic insert of 3 kb preceded by thymidine kinase and a 3′-genomic insert of 4.2 kb. The vector linearized with XhoI was electroporated into C57BL/6 ES cells. Homologous recombination in selected clones was confirmed by Southern blot with a 320-bp EcoRI–BamHI probe. βIV spectrin +/− ES cells were microinjected into C57BL/6 blastocysts to generate chimeric mice, which were bred to C57BL/6 female to produce βIV spectrin +/− F1 mice, and then βIV spectrin−/− mice by intercrossing. Mice were genotyped by PCR with primers for exon 2 of mouse βIV spectrin (forward: 5′-ACCAGGGGAAGTGGACAACAT; reverse: 5′-TGATCCGGGAGCACTCAAA) and *neo* (forward: 5′-CGTGGGATCATTGTTTTTCTCTTG; reverse: 5′-CGTGCCTCAGCCCTCCAACTATGG).

Antibodies

The NT rabbit antibody was raised against residues 15–38 in exon 2 of human βIVΣ1 spectrin. Specificity of the affinity-purified antibody was tested by immunoblot and immunocytochemistry on brain with or without a 5,000 molar excess of the antigenic peptide. The following antibodies were used: rabbit anti-βIV spectrin-SD (Berghs et al., 2001), anti-Kv1.2, and anti-caspr/paranodin (gifts of J.S. Trimmer [State University of New York, Stony Brook, NY] and J.-A. Girault [Institute du Fer à Moulin, Paris, France], respectively), mouse anti-Kv1.1 (a gift of J.S. Trimmer), anti-pan-VGSC K58/35 (Rasband et al., 1999), and anti-caspr/paranodin (Rasband and Trimmer, 2001). The following antibodies were purchased: mouse anti-ankyrin G (Zymed Laboratories), anti-β- and γ-tubulin and anti-neurofilament 200 (Sigma-Aldrich), and goat anti–rabbit and anti–mouse IgGs conjugated to Alexa 488 or 568 (Molecular Probes).

Immunoblot

Pregnant females, newborn, and adult mice were killed according to the German Animal Welfare Law. Brain tissues from E15 and E19 mouse embryos, 1- or 10-d-old mice, or adult mice were processed as described previously (Berghs et al., 2000). 50–150 μg of protein were separated by 6% SDS/PAGE and immunoblotted with primary antibodies (SD, 1:500; NT, 1:500; β-tubulin, 1:10000; γ-tubulin, 1:5,000), followed by peroxidase-conjugated goat anti–rabbit or anti–mouse IgGs (Sigma-Aldrich; 1:5,000). Signals were detected by ECL (Super Signal; Pierce Chemical Co.) with a LAS-3000 Bioimaging System (Fuji). Protein concentration was determined with the BCA assay (Pierce Chemical Co.).

Immunostaining

Anesthetized adult mice were transcardially perfused with 120 mM sodium phosphate buffer, pH 7.4, followed by 1% PFA in the same buffer at RT. Brain, optic nerves, and sciatic nerves were collected, post-fixed for an additional 1–3 h at RT, infiltrated with 30% sucrose in 120 mM sodium phosphate buffer, and frozen before cryosectioning. The labeling on 12-μm cryostat sections was performed as described previously (De Camilli et al., 1983) with anti-SD (1:50), -NT (1:50), -pan-VGSCs (1:600), -Kv1.1 (1:200), -Kv1.2 (1:400), and -caspr/paranodin (rabbit, 1:1000; mouse, 1:200) antibodies, followed by Alexa-conjugated secondary antibodies. Images were collected with a confocal microscope (model LSM 510; Carl Zeiss MicroImaging, Inc.) using Plan-Apochromat 63× or 100×/1.4 Oil DIC lenses. Image processing and morphometry were performed with the MetaMorph software (Universal Imaging Corp.). Compared images were acquired in the same conditions. For cochlea imaging, mice were killed by cervical dislocation; the inner ear was removed and fixed by immersion in 1% PFA. Next, the cochlea was dissected out, cut into three coils, and incubated overnight at 4°C with antibodies.

EM

Anesthetized βIVΣ1 −/− and +/+ mice were perfused transcardially with 2% PFA/2.5% glutaraldehyde in 0.1 M cacodylate buffer, 1 mM $CaCl_2$, pH 7.4. Optic and sciatic nerves were prepared for EM as described previously (Traka et al., 2003). Contrasted ultrathin sections were observed with an electron microscope (model EM906; Carl Zeiss MicroImaging, Inc.). Morphometry was done on 15 micrographs of sciatic nerves for each genotype. The ratio between the width of NR and juxtaparanodes [(node width/juxtaparanode width) × 100] was calculated for each NR.

ABR

Anesthetized 8-wk-old βIVΣ1 −/− mice and +/+ were exposed to tone bursts (4/6/8/12/16/24/32 kHz, 10 ms plateau with 1 ms $\cos^2$ onset and offset) or clicks of 0.03 ms generated by a System 2 (Tucker-Davis Technology) driving a high frequency speaker (Monacor). Intensities are shown as sound pressure level (dB root mean square for tone bursts, dB peak equivalent for clicks). The difference potential between vertex and mastoid was amplified (factor 5e4), filtered (low pass: 4 kHz, high pass: 100 Hz), and sampled into System 2 at a rate of 50 kHz. Stimuli were presented 2,000 times at 20 Hz. The EEG was recorded for 20 ms and averaged (2 × 2,000 traces) to obtain two mean ABR traces for sound intensity. ABR latencies were analyzed after stimulation with 80-dB clicks, and the thresholds were estimated with a 10-dB precision by visual inspection. In some experiments, stimuli at 20 and 90 Hz and a recording time of 10 ms were used to compare the latency of wave IV on presentation of click stimuli at various intensities at slow and rapid stimulation rates.

Statistics

Statistics were performed with Sigma Stat 3.0 (SPSS Inc.). Data are reported as means ± SEM and compared using the unpaired Mann and Whitney U test for the immunostaining measurements and *t* test for the EM and ABR.

We thank the following people for their help: L. Alexopoulou, S. Anderson, S. Bramke, L. Duclos, R. Flavell, R. Funk, U. Hönicke, W. John, D. Khimich, K. Knoch, C. Lafont, C. Lorra, H. Mziaut, U. Nimtschke, C. Nizak, J. Ouwendjik, F. Perez, K. Pfriem, D. Streichert, P. Verkade, M. Wilsch-Brauuninger, and C. Zeiss.

This work was supported by grants from the Alexander von Humboldt Foundation (M. Solimena), the National Institutes of Health (M. Solimena and M.N. Rasband), the American Diabetes Association (M. Solinema), the Wadsworth Foundation (M.N. Rasband), the Deutsche Forschungsgemeinschaft and the Max Planck Gesellschaft (T. Moser), and the European Commission (E. Scarfone).

Submitted: 2 August 2004
Accepted: 12 August 2004

References

Bennett, V., and P.J. Stenbuck. 1979. Identification and partial purification of ankyrin, the high affinity membrane attachment site for human erythrocyte spectrin. *J. Biol. Chem.* 254:2533–2541.

Bennett, V., and A.J. Baines. 2001. Spectrin and ankyrin-based pathways: metazoan inventions for integrating cells into tissues. *Physiol. Rev.* 81:1353–1392.

Berghs, S., D. Aggujaro, R. Dirkx Jr., E. Maksimova, P. Stabach, J.M. Hermel, J.P. Zhang, W. Philbrick, V. Slepnev, T. Ort, and M. Solimena. 2000. βIV spectrin, a new spectrin localized at axon initial segments and nodes of ranvier in the central and peripheral nervous system. *J. Cell Biol.* 151:985–1002.

Berghs, S., F. Ferracci, E. Maksimova, S. Gleason, N. Leszczynski, M. Butler, P. De Camilli, and M. Solimena. 2001. Autoimmunity to βIV spectrin in paraneoplastic lower motor neuron syndrome. *Proc. Natl. Acad. Sci. USA.* 98:6945–6950.

De Camilli, P., R. Cameron, and P. Greengard. 1983. Synapsin I (protein I), a nerve terminal-specific phosphoprotein. I. Its general distribution in synapses of the central and peripheral nervous system demonstrated by immunofluorescence in frozen and plastic sections. *J. Cell Biol.* 96:1337–1354.

De Matteis, M.A., and J.S. Morrow. 2000. Spectrin tethers and mesh in the biosynthetic pathway. *J. Cell Sci.* 113:2331–2343.

Hood, J.D. 1950. Studies in auditory fatigue and adaptation. *Acta Otolaryngol. Suppl.* 92:1–57.

Jenkins, S.M., and V. Bennett. 2001. Human auditory evoked potentials: possible brain stem components detected on the scalp. *Science.* 167:1517–1518.

Jewett, D.L., M.N. Romano, and J.S. Williston. 1970. Human auditory evoked potentials: possible brain stem components detected on the scalp. *Science.* 167:1517–1518.

Komada, M., and P. Soriano. 2002. βIV-spectrin regulates sodium channel clustering through ankyrin-G at axon initial segments and nodes of Ranvier. *J. Cell Biol.* 156:337–348.

Marchesi, V.T. 1985. Stabilizing infrastructure of cell membranes. *Annu. Rev. Cell Biol.* 1:531–561.

Marchesi, V.T., and E. Steers Jr. 1968. Selective solubilization of a protein component of the red cell membrane. *Science.* 159:203–204.

Parkinson, N.J., C.L. Olsson, J.L. Hallows, J. McKee-Johnson, B.P. Keogh, K. Noben-Trauth, S.G. Kujawa, and B.L. Tempel. 2001. Mutant β-spectrin 4 causes auditory and motor neuropathies in quivering mice. *Nat. Genet.* 29:61–65.

Poliak, S., and E. Peles. 2003. The local differentiation of myelinated axons at nodes of Ranvier. *Nat. Rev. Neurosci.* 4:968–980.

Rasband, M.N., and J.S. Trimmer. 2001. Subunit composition and novel localization of K^+ channels in spinal cord. *J. Comp. Neurol.* 429:166–176.

Rasband, M.N., E. Peles, J.S. Trimmer, S.R. Levinson, S.E. Lux, and P. Shrager. 1999. Dependence of nodal sodium channel clustering on paranodal axoglial contact in the developing CNS. *J. Neurosci.* 19:7516–7528.

Robertson, J.D. 1957. The ultrastructure of nodes of Ranvier in frog nerve fibres. *J. Physiol.* 137:8–9.

Salzer, J.L. 2003. Polarized domains of myelinated axons. *Neuron.* 40:297–318.

Suter, U., and S.S. Scherer. 2003. Disease mechanisms in inherited neurophathies. *Nat. Rev. Neurosci.* 4:714–726.

Traka, M., L. Goutebroze, N. Denisenko, M. Bessa, A. Nifli, S. Havaki, Y. Iwakura, F. Fukamauchi, K. Watanabe, B. Soliven, et al. 2003. Association of TAG-1 with Caspr2 is essential for the molecular organization of juxtaparanodal regions of myelinated fibers. *J. Cell Biol.* 162:1161–1172.

Tse, W.T., J. Tang, O. Jin, C. Korsgren, K.M. John, A.L. Kung, B. Gwynn, L.L. Peters, and S.E. Lux. 2001. A new spectrin, βIV, has a major truncated isoform that associates with promyelocytic leukemia protein nuclear bodies and the nuclear matrix. *J. Biol. Chem.* 276:23974–23985.

Zimmermann, H. 1996. Accumulation of synaptic vesicle proteins and cytoskeletal specializations at the peripheral node of Ranvier. *Microsc. Res. Tech.* 34: 462–473.